Soil Dynamics and Earthquake Engineering 99 (2017) 108–123

Contents lists available at ScienceDirect

Soil Dynamics and Earthquake Engineering

journal homepage: www.elsevier.com/locate/soildyn

Numerical modelling of micro-seismic and infrasound noise radiated by a wind turbine

Theodore V. Gortsas[a,b], Theodoros Triantafyllidis[a], Stylianos Chrisopoulos[a], Demosthenes Polyzos[b,*]

[a] Institute of Soil Mechanics and Rock Mechanics Karlsruhe Institute of Technology (KIT), 76128 Karlsruhe, Germany
[b] Department of Mechanical Engineering & Aeronautics, University of Patras, Patras GR-26500, Greece

ARTICLE INFO

Keywords:
Wind turbines
Infrasound noise
Micro-seismicity
Fluid structure interaction
Boundary element method
Large-scale problems
ACA/BEM

ABSTRACT

Infrasound, low frequency noise and soil vibrations produced by large wind turbines might disturb the comfort of nearby structures and residents. In addition repowering close to urban areas produces some fears to the nearby residents that the level of disturbance may increase. Due to wind loading, the foundation of a wind turbine interacts with the soil and creates micro-seismic surface waves that propagate for long distances and they are able to influence adversely sensitive measurements conducted by laboratories located far from the excitation point. A numerical study on the creation and propagation of those waves to the surrounding area is the subject of the present work. Besides, the contribution of those waves to airborne sound generated by the soil-air interaction is also investigated. All numerical simulations are performed with the aid of the Boundary Element Method (BEM), which is ideal for solving such problems since it takes automatically into account the radiation conditions of the waves and thus only the soil-foundation interface and the free surface of the surrounding soil are needed to be discretized. Foundation and soil are considered as linearly elastic materials with interfacial bonding. The frequency domain Helmholtz equation is employed for the simulation of acoustic waves. Numerical results dealing with the airborne and soil borne noise propagation and attenuation are presented and disturbances that might be caused to nearby and far-field structures are discussed.

1. Introduction

The last 35 years, significant progress has been made on the design of offshore and onshore wind turbines (WT) rendering the exploitation of wind power as one of the most fastest-growing renewable energy sources [9,4]. However, as WTs become bigger and more powerful many problems dealing with the disturbance of the surrounding environment due to installation and operation of wind farms have been reported [1,16,40,6]. Focusing on onshore WTs, the most usual complaint is that they are noisy.

WTs emit broadband sound, which may be audible in distances of 300–1000 m and annoying particularly because of its pulsating character. Infrasound, which corresponds to frequencies below 20 Hz is inaudible by human ears, but may produce a feeling of static pressure and periodic masking effects for high-pressure levels. Infrasound and low frequency sound have very low absorption in the atmosphere; it can propagate for long distances from a WT and is higher for large WTs than for small ones. Besides, near to the ground level are positively affected by the presence of the ground, the atmospheric refraction and the temperature gradient of the atmosphere. Due to the greater impedance of the soil with respect to air, the ground reflects most of the energy of an incident sound wave and a receiver is influenced by both the direct and the reflected sound. Atmospheric refraction is the upward or downward change of sound propagation direction because of the sound speed gradient near to the ground. For humans, animals and structures being close to a WT, the atmospheric refraction effect can be ignored. However, for distances larger than 100 m and in cases where both source and receiver are close to the ground surface, the influence of atmospheric refraction on the infrasound level is significant. On the other hand the temperature gradient near to ground level affects the speed of the propagating sound. At night hours, the cooling of the ground is faster than the corresponding one in the atmosphere causing higher sound speeds and downward bending of the propagation direction of infrasound. A plethora of published papers and reports can be found on the subject, some representatives are those of Manley et al. [19], Møller and Pedersen [24], [39], Öhlund and Larsson [26], Jakobsen [12], Turnbull et al. [38], Kelley et al. [15], Zajamšek et al. [46], Hoffmeyer and Jakobsen [10], Pedersen et al. [27], Keith et al. [14], Carman [7], Michaud et al. [21,22], Marcillo et al. [20], Katinas et al. [13] and Pilger and Ceranna [28].

* Corresponding author.

http://dx.doi.org/10.1016/j.soildyn.2017.05.001
Received 21 March 2017; Received in revised form 2 May 2017; Accepted 3 May 2017
Available online 16 May 2017

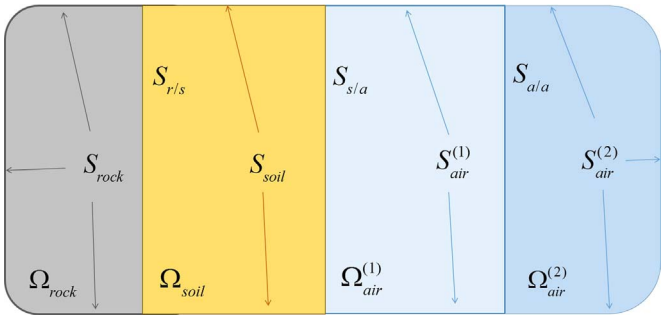

Fig. 1. Representation of the elastic and acoustic interacting domains.

In the majority of the published papers, reports, conference proceedings and books on the subject, the main sources responsible for emitting low frequency noise by a WT are of aerodynamic nature coming from blade vortex interaction, turbulent inflow noise, blade tower interaction and blade tip turbulent flow [23,25,42]. Secondary cause is the infrasound generated by the rotor and other rotating mechanical parts in the nacelle of a WT [2]. Møller and Pedersen [24] give a thorough review on the effects of that infrasound emission on the nearby inhabitants and they report that "*The infrasonic part of the spectrum was below the normal hearing threshold in all investigated cases of complaints, but it was said to cause perceptible vibrations and rattling of windows and wall-mounted objects, which contributed to negative reactions to wind turbine noise*", which means that the observed structural vibrations are attributed to the interaction of infrasound and low frequency sound with the nearby buildings. Furthermore, Styles and co-workers reported micro-seismic waves (0.1–10 Hz) generated by the vibrational modes of the tower of a WT and propagated through the ground for very long distances [31,32,36,37]. The lower the frequency the longer the distance that such micro-seismic disturbances become detectable. According to Styles observations, those micro-seismic waves have been detected by the Eskdalemuir station at Scotland on the seismometers buried in the ground many kilometers away from wind farms, even in the presence of significant levels of background seismic noise. Saccorotti et al. [34] reach to the same conclusions for measurements carried out in the vicinity of Virgo, the Italian–French gravitational wave observatory located close to Pisa in Italy. Very recently, Stammler and Ceranna [35] confirm the findings of Styles and Saccorotti by comparing the seismic records in the Gräfenberg array of Germany before and after the installation of WTs in the area. More precisely, they report that station sites with WTs within distances up to 5 km are exposed to significant disturbances, while those signals have been also detected in distances above 15 km. Consequently, the questions here is first, how important is the contribution of those micro-seismic waves to the detected structural vibrations of nearby houses and second, do they produce appreciable infrasound at the surrounding environment of a WT? To the authors' best knowledge, the contribution of those micro-seismic waves to the perceptible structural vibrations (soil-structure interaction) and the background low frequency noise (soil-air interaction) has not reported so far in the literature.

The goal of the present work is to simulate the propagation of infrasound and micro-seismic disturbances produced by a WT both in soil and air and to compare their influence inside and outside of a simple room located at 500 m distance from a WT. First, the seismic waves generated by the vibrations of a WT will be simulated by considering 3D axisymmetric foundation subjected to a bending moment as well as to vertical and horizontal forces imposed by the vibration of WT's tower due to the wind action and turbine interaction. Since most of those seismic waves spread as Rayleigh waves and taking into account that infrasound and low frequency sound emitted by a WT attenuate as cylindrical waves [18], it is apparent that one can investigate the associated acoustic and elastic wave propagation problems via two dimensional considerations without significant error and with high computational gain. Although the analytical models employed in simulations do not describe exactly the real world, they give valuable information on the noise assessment and enable one to perform extensive parametric studies which otherwise would require expensive and time-consuming experiments to be conducted.

Table 2
Geometrical details and material properties for the model shown in Fig. 9.

Region	Material Properties	Geometrical Characteristics
Soil	Density: $\rho = 1800$ kg/m^3 Young Modulus: $E = 4.050 \times 10^8$ N/m^2 Poisson Ratio: $\nu = 0.25$	$H_s = 100$ m
Bedrock	Density: $\rho = 2600$ kg/m^3 Young Modulus: $E = 32 \times 10^9$ N/m^2 Poisson Ratio: $\nu = 0.23$	$H_2 = L_1 * \tan(\beta)$ $L = 100$ m, $L_0 = 200$ m, $L_1 = 200$ m, $L_2 = 200$ m, $L_3 = 200$ m
Air at 0 °C	Density: $\rho = 1.2922$ kg/m^3 Sound velocity: $c = 331.30$ m/s	$H_0 = 350$ m, $H_1 = 150$ m
Air at 10 °C	Density: $\rho = 1.2466$ kg/m^3 Sound velocity: $c = 337.31$ m/s	Semi-infinite
Air at 20 °C	Density: $\rho = 1.2041$ kg/m^3 Sound velocity: $c = 343.21$ m/s	Square (6.60 m)x(6.60 m)
Foundation of WT	Density: $\rho = 2500$ kg/m^3 Young Modulus: $E = 39 \times 10^9$ N/m^2 Poisson Ratio: $\nu = 0.2$	$H_w = 2.97$ m, $L_w = 19.8$ m
Structure at 500 m from WT	Density: $\rho = 2500$ kg/m^3 Young Modulus: $E = 39 \times 10^9$ N/m^2 Poisson Ratio: $\nu = 0.2$	$H_h = 7$ m, $h_h = 2.0$ m

Table 1
Displacements at different distances from the WT foundation for excitation frequencies 1 Hz, 5 Hz and 10 Hz.

Excitation	Displacement at 300 m	Displacement at 500 m	Displacement at 1000 m	Displacement at 5000 m	Displacement at 10,000 m
Axial Force at 1 Hz ($n = 0.9$)	6.32845×10^{-7} m	3.9960×10^{-7} m	2.14144×10^{-7} m	5.030×10^{-8} m	2.6959×10^{-8} m
Axial Force at 5 Hz ($n = 0.6$)	1.29338×10^{-6} m	9.5195×10^{-7} m	6.2805×10^{-7} m	2.3912×10^{-7} m	1.5776×10^{-7} m
Axial Force at 10 Hz ($n = 0.55$)	1.09915×10^{-6} m	8.2992×10^{-7} m	5.6685×10^{-7} m	2.3390×10^{-7} m	1.5976×10^{-7} m
Shear Force at 1 Hz ($n = 1$)	1.91162×10^{-6} m	1.1469×10^{-6} m	5.7348×10^{-7} m	1.1469×10^{-7} m	5.7348×10^{-8} m
Shear Force at 5 Hz ($n = 0.90$)	4.2103×10^{-6} m	2.6586×10^{-6} m	1.42469×10^{-6} m	3.3469×10^{-7} m	1.7936×10^{-7} m
Shear Force at 10 Hz ($n = 0.90$)	4.73724×10^{-6} m	2.9913×10^{-6} m	1.6030×10^{-6} m	3.7658×10^{-7} m	2.0180×10^{-7} m
Bending Moment at 1 Hz ($n = 2$)	5.27484×10^{-6} m	1.8989×10^{-6} m	4.7473×10^{-7} m	1.8989×10^{-8} m	4.7473×10^{-9} m
Bending Moment at 5 Hz ($n = 0.8$)	4.78255×10^{-5} m	3.1782×10^{-5} m	1.8254×10^{-5} m	5.0371×10^{-6} m	2.8930×10^{-6} m
Bending Moment at 10 Hz ($n = 0.65$)	9.31739×10^{-5} m	6.6849×10^{-5} m	4.2601×10^{-5} m	1.4965×10^{-5} m	9.5372×10^{-6} m

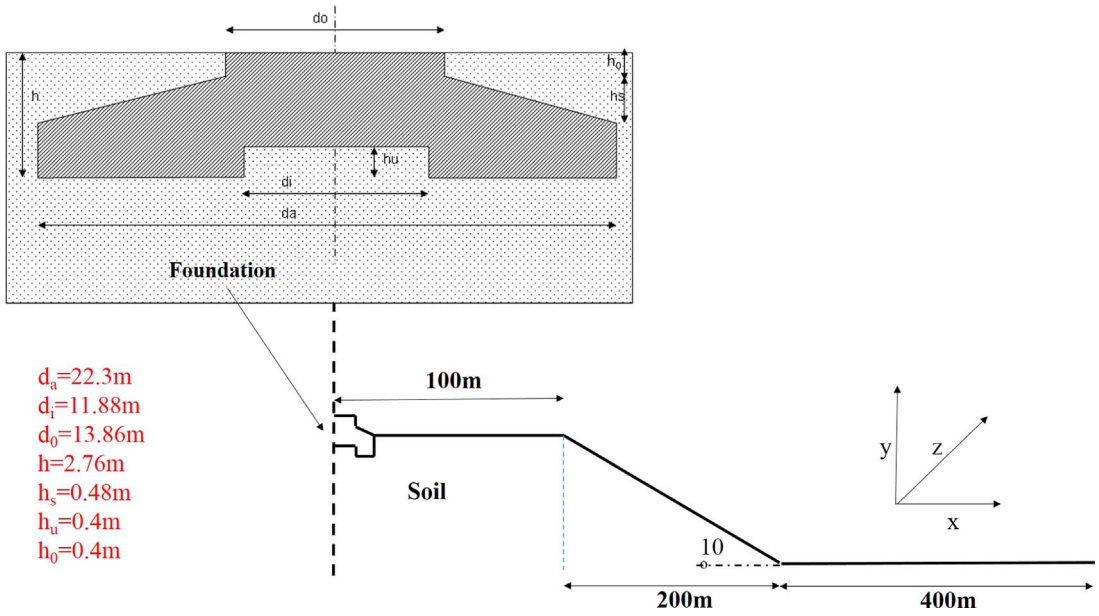

Fig. 2. An axisymmetric cross-section of the 3D geometry of the problem and dimensions for the circular foundation.

It is well known that multiple reflections of sound waves by complicated geometries and soil-air, soil-structure interactions cannot be calculated with simple engineering tools and shifting should be made to numerical methods. A robust numerical tool for solving acoustic, elastic and fluid-structure interaction problems like the aforementioned ones is the Boundary Element Method (BEM) [3,29]. Two remarkable advantages it offers as compared to the Finite Element Method is the reduction of the dimensionality of the problem by one and its high solution accuracy. Despite its advantages, the brutal application of BEM to large-scale problems suffers from very time consuming computations and high demands for computer memory capacity. Both problems come from the full populated and non-symmetric matrix coefficient [A] of the final system of algebraic equations [A]{x}={b} that the BEM solves in order to calculate the unknown vector {x}. This drawback confines the application of the BEM to problems with no more than 80,000 degrees of freedom (dofs), utilizing double precision complex numbers, in a computer with 100 GB RAM. A very efficient methodology that circumvents that problem and accelerates remarkably the solution process of a BEM code is the effective combination of Hierarchical Matrices (HM), Adaptive Cross Approximation (ACA) techniques and iterative solvers (e.g. GMRES) as it is explained in Gortsas et al. [8]. That ACA/BEM is employed in the present work for the numerical solution of the aforementioned wave propagation problems.

The paper is structured as follows: in the next section the ACA/BEM for solving fluid-structure and soil-structure interaction problems is reported in brief. In Section 3 the seismic waves generated by the vibrations of a WT will be simulated by considering 3D axisymmetric foundation subjected to a bending moment as well as to vertical and horizontal forces imposed by the vibration of WT's tower. Based on those results, the determination of the bending, vertical and horizontal excitations used for the 2D simulations of the next section is accomplished. In Section 4 the propagation of infrasound and micro-seismic disturbances produced by a WT both in soil and air is simulated and their influence inside and outside of a simple room located 500 m far from a WT is assessed. Finally, Section 5 consists of the conclusions pertaining to this work.

2. An advanced ACA/BEM for solving acoustic-structure and soil-structure interaction problems

In this section the ACA/BEM utilized for the solution of the acoustic-structure and soil-structure interaction problems of the present work is explained in brief. The method is illustrated in frequency domain since most of the signal generated by a wind turbine is either periodic or transient with relatively short duration. In the later case the transient signal is converted to the frequency domain by means of the Fast Fourier Transform (FFT) and the corresponding boundary value problems are solved for each frequency of the spectrum by the frequency domain ACA/BEM explained below. The obtained results are shifted to time domain again through a standard inverse FFT algorithm [41].

Consider the consequence of interacting materials shown in Fig. 1. Rock and soil are considered as linear elastic materials, a hypothesis which is also justified by measurements due to the very small amplitudes and strains, while two acoustical regions consisting of air at two different temperatures follow the soil region. The material properties of all regions are given in Table 2. The rock-soil, soil-air$^{(1)}$ and air$^{(1)}$-air$^{(2)}$ interfaces are symbolized as $S_{r/s}$, $S_{s/a}$ and $S_{a/a}$, respectively.

For a dynamic problem in frequency domain elastic displacement vectors $\mathbf{u}$ and acoustic pressures p of all regions satisfy the following partial differential equations:

$$\mu_{rock}\nabla^2\mathbf{u}^{rock}(\mathbf{x}) + (\lambda_{rock} + \mu_{rock})\nabla\nabla\cdot\mathbf{u}^{rock}(\mathbf{x}) + \rho_{rock}\omega^2\mathbf{u}^{rock}(\mathbf{x}) = \mathbf{0},\ \mathbf{x}\in\Omega_{rock} \tag{1}$$

$$\mu_{soil}\nabla^2\mathbf{u}^{soil}(\mathbf{x}) + (\lambda_{soil} + \mu_{soil})\nabla\nabla\cdot\mathbf{u}^{soil}(\mathbf{x}) + \rho_{soil}\omega^2\mathbf{u}^{soil}(\mathbf{x}) = \mathbf{0},\ \mathbf{x}\in\Omega_{soil} \tag{2}$$

$$\nabla^2 p^{air(1)}(\mathbf{x}) + \left(\frac{\omega}{c^{air(1)}}\right)^2 p^{air(1)}(\mathbf{x}) = 0,\ \mathbf{x}\in\Omega_{air}^{(1)} \tag{3}$$

$$\nabla^2 p^{air(2)}(\mathbf{x}) + \left(\frac{\omega}{c^{air(2)}}\right)^2 p^{air(2)}(\mathbf{x}) = 0,\ \mathbf{x}\in\Omega_{air}^{(2)} \tag{4}$$

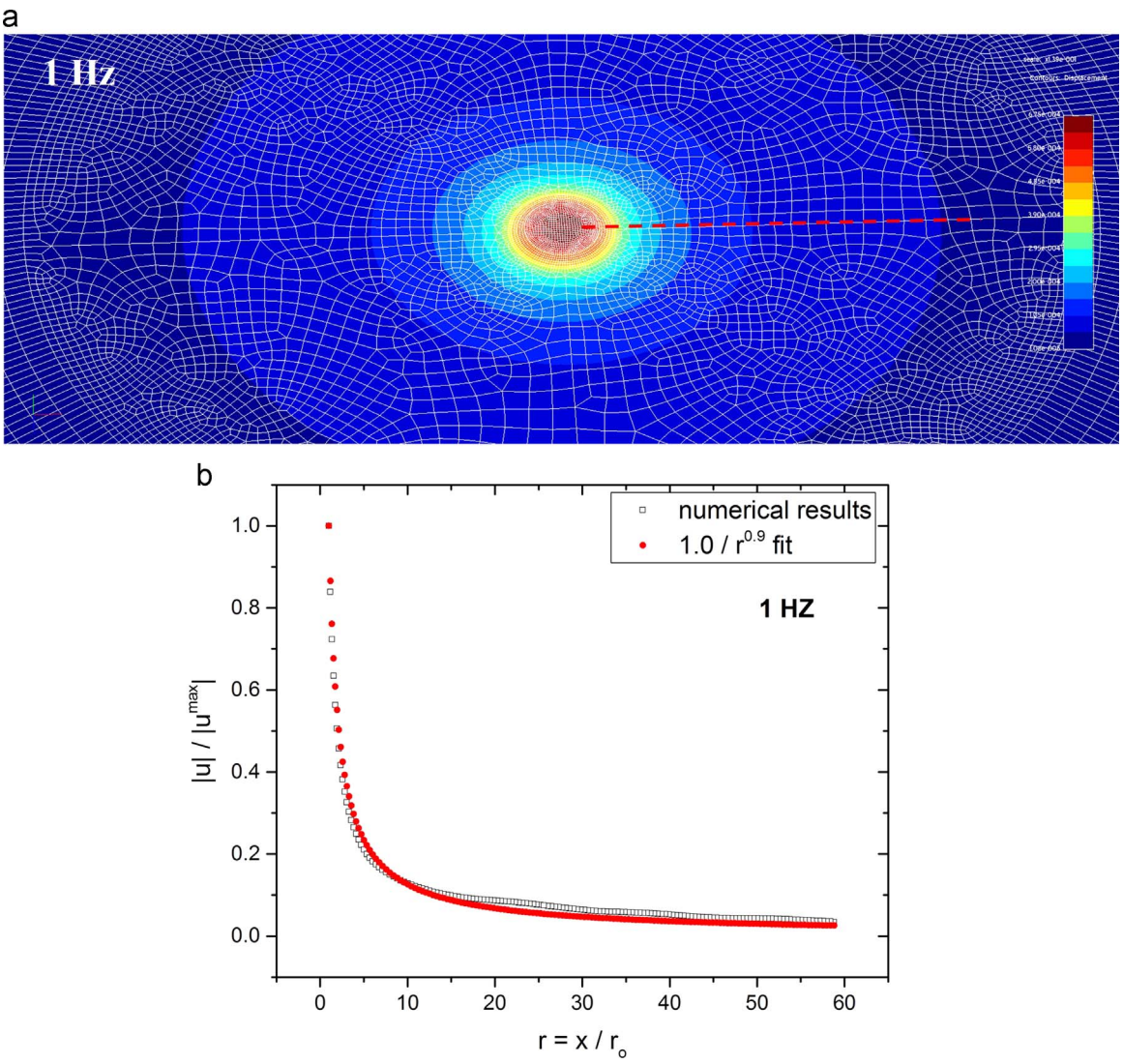

Fig. 3. (a) Contour map of vertical displacements around the WT's foundation derived by a vertical traction loading of t = 1.180 kPa at the frequency of 1 Hz. (b) The displacement decay of the generated waves normalized by the maximum displacement appearing at the soil-foundation interface. The horizontal distance from the WT is normalized by the radius of the foundation $r_o = d_a/2$. The red dotted line indicates that the generated harmonic waves across the line depicted in Fig. 3(a) decay as $1/r^{0.9}$.

where λ, μ represent the Lamé constants of the regions occupied by elastic bodies, ρ the mass density, ω the frequency and c the phase velocity of sound waves propagating in air.

At the interfaces of all regions the following boundary conditions should be satisfied

$$\left.\begin{aligned} \mathbf{u}^{rock} &= \mathbf{u}^{rock} \\ \mathbf{t}^{rock} &= -\,\mathbf{t}^{soil} \end{aligned}\right\} \mathbf{x} \in S_{r/s} \tag{5}$$

$$\left.\begin{aligned} \frac{1}{\omega^2 \rho^{air(1)}} \partial_n p^{air(1)} &= -\,\hat{\mathbf{n}} \cdot \mathbf{u}^{soil} \\ p^{air(1)} &= \hat{\mathbf{n}} \cdot \mathbf{t}^{soil} \end{aligned}\right\} \mathbf{x} \in S_{s/a} \tag{6}$$

$$\left.\begin{aligned} p^{air(1)} &= p^{air(2)} \\ \frac{1}{\rho^{air(1)}} \partial_n p^{air(1)} &= -\,\frac{1}{\rho^{air(2)}} \partial_n p^{air(2)} \end{aligned}\right\} \mathbf{x} \in S_{a/a} \tag{7}$$

where $\mathbf{t}$ stands for elastic traction vector at a surface with unit normal vector $\hat{\mathbf{n}}$ and $\partial_n p$ represents the pressure flux at the interfaces $S_{s/a}$ and $S_{a/a}$ with $\hat{\mathbf{n}}$ being their normal vector.

Instead of solving the differential Eq. (1–4) the following integral representations for the displacements and pressures of the just described problem can be used within the formalism of the boundary integral equations [29,45,5].

$$c^{rock}(\mathbf{x})\,\mathbf{u}^{rock}(\mathbf{x}) + \int_{S_{rock}+S_{r/s}} \widetilde{\mathbf{T}}^{rock}(\mathbf{x},\mathbf{y})\,\mathbf{u}^{rock}(\mathbf{y})\,dS_y = \int_{S_{rock}+S_{r/s}} \widetilde{\mathbf{U}}^{rock}(\mathbf{x},\mathbf{y})\,\mathbf{t}^{rock}(\mathbf{y})\,dS_y \tag{8}$$

$$c^{soil}(\mathbf{x})\,\mathbf{u}^{soil}(\mathbf{x}) + \int_{S_{soil}+S_{r/s}+S_{s/a}} \widetilde{\mathbf{T}}^{soil}(\mathbf{x},\mathbf{y})\,\mathbf{u}^{soil}(\mathbf{y})\,dS_y = \int_{S_{soil}+S_{r/s}+S_{s/a}} \widetilde{\mathbf{U}}^{soil}(\mathbf{x},\mathbf{y})\,\mathbf{t}^{soil}(\mathbf{y})\,dS_y \tag{9}$$

$$c^{air(1)}(\mathbf{x})\,p^{air(1)}(\mathbf{x}) + \int_{S^{(1)}_{air}+S_{s/a}+S_{a/a}} \partial_n G^{air(1)}(\mathbf{x},\mathbf{y})\,p^{air(1)}(\mathbf{y})\,dS_y = \int_{S^{(1)}_{air}+S_{s/a}+S_{a/a}} G^{air(1)}(\mathbf{x},\mathbf{y})\,\partial_n p^{air(1)}(\mathbf{y})\,dS_y \tag{10}$$

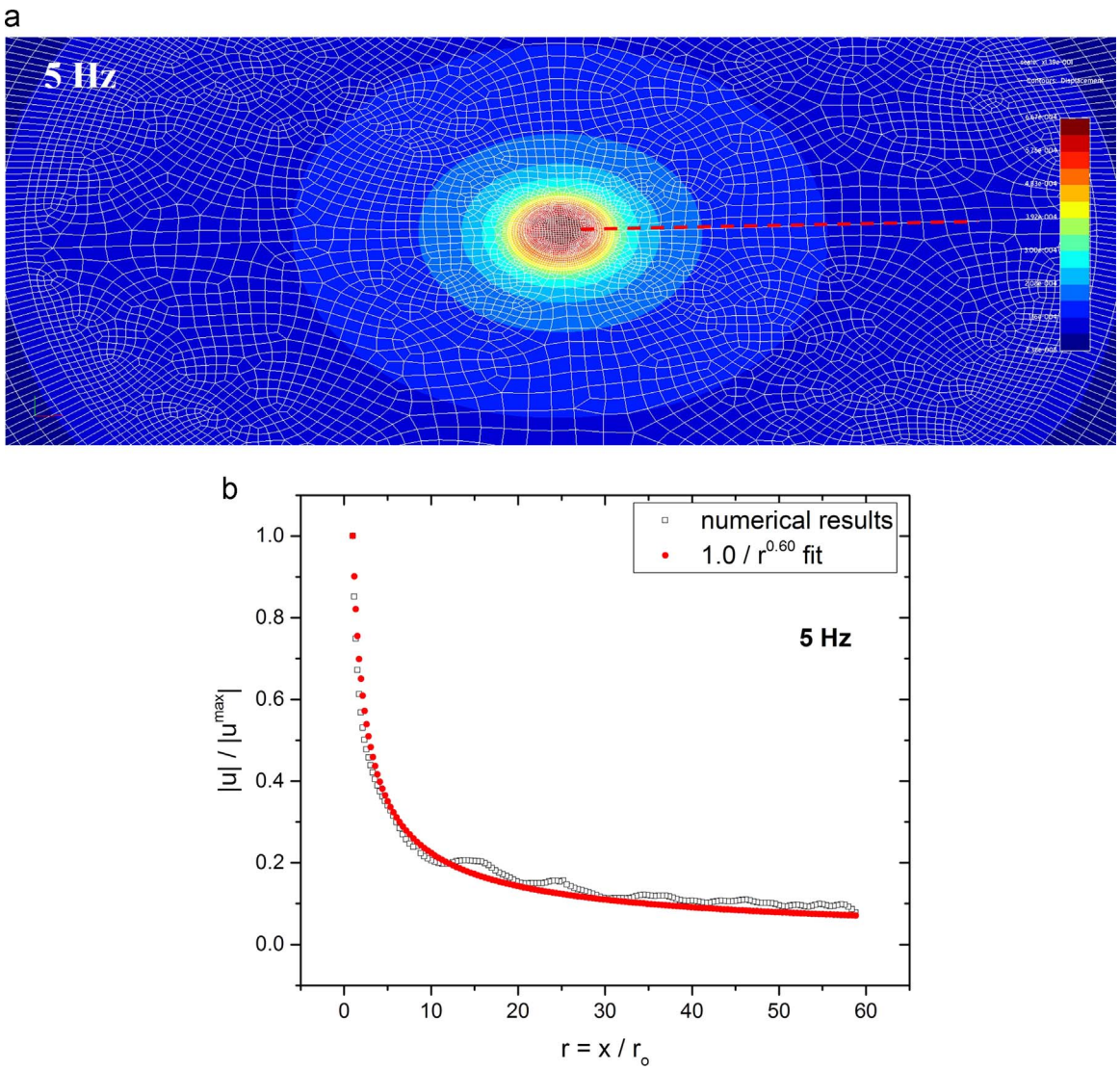

Fig. 4. The same as in Fig. 3 for the excitation frequency of 5 Hz. In the line shown in Fig. 4(a), the vertical displacement of the soil decays as $1/r^{0.6}$.

$$c^{air(2)}(\mathbf{x})\, p^{air(2)}(\mathbf{x}) + \int_{S^{(2)}_{air}+S_{a/a}} \partial_n G^{air(2)}(\mathbf{x},\mathbf{y})\, p^{air(2)}(\mathbf{y})\, dS_y = \int_{S^{(2)}_{air}+S_{a/a}} G^{air(2)}(\mathbf{x},\mathbf{y})\, \partial_n p^{air(2)}(\mathbf{y})\, dS_y \tag{11}$$

where $\widetilde{\mathbf{U}}$, G are the fundamental solutions of the Navier-Cauchy Eqs. (1), (2) and the Helmholtz Eqs. (3), (4), respectively, $\widetilde{\mathbf{T}}$ and $\mathbf{t}$ are the traction fields corresponding to elastic fundamental solution $\widetilde{\mathbf{U}}$ and displacement $\mathbf{u}$, ∂_n denotes derivative across the unit vector being normal to the boundary of the corresponding region, while the coefficient $c(\mathbf{x})$ takes the values 0, 1 and 0.5 when $\mathbf{x}$ lies inside, outside and at the boundary of the region of interest, respectively.

According to a conventional BEM formulation, all the boundaries and interfaces of the correlated regions are discretized into three-nodded quadratic or two-nodded linear isoparametric line boundary elements and after the application of the integral Eq. (8–11) at the corresponding nodes, one obtains the following linear systems of algebraic equations, respectively

$$\left[\widetilde{\mathbf{T}}^{rock}\right]\cdot\{\mathbf{u}^{rock}\} = [\widetilde{\mathbf{U}}^{rock}]\{\mathbf{t}^{rock}\} \tag{12}$$

$$\left[\widetilde{\mathbf{T}}^{soil}\right]\cdot\{\mathbf{u}^{soil}\} = [\widetilde{\mathbf{U}}^{soil}]\{\mathbf{t}^{soil}\} \tag{13}$$

$$[\widetilde{\mathbf{Q}}^{air(1)}]\cdot\{\mathbf{p}^{air(1)}\} = [\widetilde{\mathbf{G}}^{air(1)}]\{\mathbf{q}^{air(1)}\} \tag{14}$$

$$[\widetilde{\mathbf{Q}}^{air(2)}]\cdot\{\mathbf{p}^{air(2)}\} = [\widetilde{\mathbf{G}}^{air(2)}]\{\mathbf{q}^{air(2)}\} \tag{15}$$

where $\{\mathbf{u}^{rock}\}$, $\{\mathbf{t}^{rock}\}$ and $\{\mathbf{u}^{soil}\}$, $\{\mathbf{t}^{soil}\}$ are vectors containing the nodal values of displacements and tractions belonging to the surface elements discretizing the boundaries of the regions Ω_{rock}, Ω_{soil}, respectively, $\{\mathbf{p}^{air(1)}\}$, $\{\mathbf{q}^{air(1)}\}$ and $\{\mathbf{p}^{air(2)}\}$, $\{\mathbf{q}^{air(2)}\}$ are the vectors with the nodal values of pressures and their fluxes corresponding to surface elements discretizing the boundaries of the regions $\Omega^{(1)}_{air}$, $\Omega^{(2)}_{air}$, respectively. The matrices contain regular and singular integrals evaluated with high accuracy as it is explained in Polyzos et al. [29] and Agnantiaris and Polyzos [3].

Combing Eqs. (12), (13), (14) and (15) via the interfacial conditions (5)-(7) and rearranging one obtains a well posed system of linear algebraic equations of the general form:

$$[\mathbf{A}]\cdot\{\mathbf{X}\} = \{\mathbf{B}\} \tag{16}$$

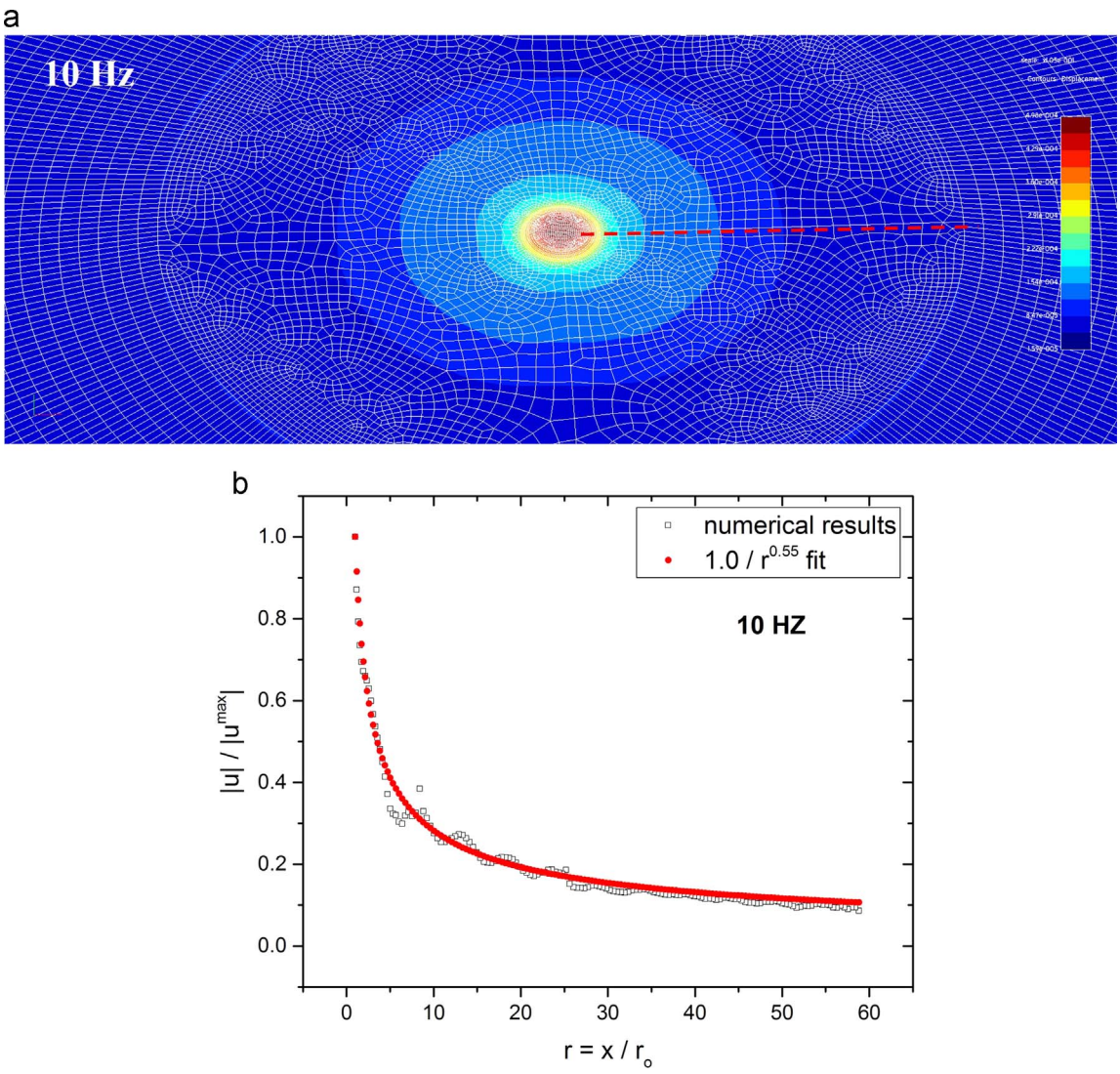

Fig. 5. The same as in Fig. 3 for the frequency of 10 Hz. In the line shown in Fig. 5(a), the vertical displacement of the soil decays as $1/r^{0.55}$.

where the vectors {**X**} and {**B**} contain all the unknown and known nodal components of the boundary fields, respectively.

As it has been already mentioned in the introduction, in conventional BEM, [**A**] is a full populated matrix requiring $O(N^2)$ operations for its buildup and $O(N^3)$ operations for the solution of Eq. (16) via typical LU-decomposition solvers, which is prohibitive for solving realistic problems where the degrees of freedom N are of the order of hundreds of thousands.

In the present work, in order to overcome the conventional BEM memory limitations and solve the above described problem for a large number of elements, a hierarchical ACA accelerated BEM has been utilized. More precisely, the matrix [**A**] appearing in Eq. (16) is represented hierarchically by using a block tree structure. By means of simple geometric considerations the blocks, which correspond to large distances between source and collocation points, are characterized as far field blocks (or admissible). These blocks which are assembled in general from entries of the matrix pairs $\left[\widetilde{\mathbf{T}}^{rock}\right][\widetilde{\mathbf{U}}^{rock}]$ and $\left[\widetilde{\mathbf{T}}^{soil}\right][\widetilde{\mathbf{U}}^{soil}]$ of Eqs. (12) and (13), respectively as well as the matrices $[\widetilde{\mathbf{Q}}^{air(1)}]$, $[\widetilde{\mathbf{G}}^{air(1)}]$ and $[\widetilde{\mathbf{Q}}^{air(2)}]$, $[\widetilde{\mathbf{G}}^{air(2)}]$ of Eqs. (14) and (15) are compressed using low rank matrices found by an ACA algorithm [8]. The remaining blocks of the tree, which are dominated by the singular behavior of the fundamental displacement and traction kernels, are characterized as near field blocks (or non-admissible) and are fully calculated as in conventional BEM. Furthermore, a significant reduction of the solution time of the problem is accomplished by utilizing the iterative solver GMRES [33] for the solution of Eq. (16). For the faster convergence of the GMRES solution a right preconditioner has been used by either considering a block diagonal preconditioner, or by utilizing a low accuracy hierarchical LU decomposition of the matrix [**A**]. More details on the aforementioned ACA/BEM technique can be found in Gortsas et al. [8].

3. 3-D simulations for micro-seismicity caused by the vibrations of a WT

The goal of the present section is to simulate the micro-seismic waves generated by the bending, vertical and horizontal vibrations of a

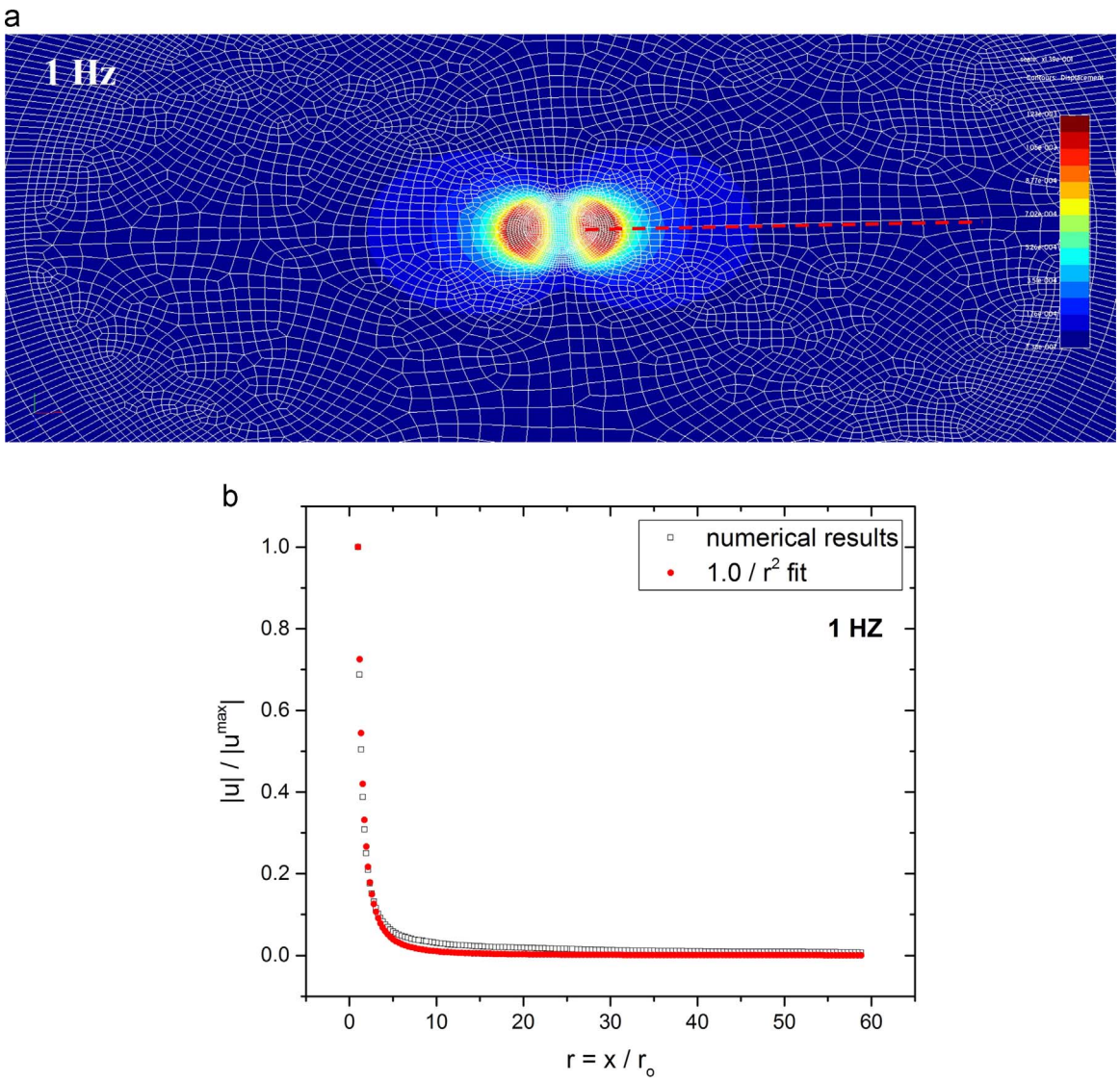

Fig. 6. (a) Contour map of vertical displacements around the WT's foundation derived by a moment loading of M = 78.202 MNm at the frequency of 1 Hz. (b) The decay of vertical displacements normalized by the maximum displacement appearing at the soil-foundation interface versus radial distance r. The horizontal distance from the WT is normalized by the radius of the foundation $r_o = d_a/2$. In the line shown in Fig. 3(a), the vertical displacement of the soil surface decays as $1/r^2$.

WT and to examine their decay rate in dependence form the distance of the vibrating WT. In order to choose realistic inputs for our simulations we exploit the information being available in the literature concerning measurements on the propagation of ground-borne noise generated by WTs. Styles and co-workers [31,32,36,37] after many observations and measurements with seismometers buried in the ground many kilometers away from wind farms, reached to the following conclusions: (a) WTs generate low frequency ground vibrations the amplitude of which increases with wind speed; (b) The main window of the Fourier spectrum for these vibrations is between 0.4 Hz and 10 Hz, while sharp picks appear at the axial, torsional and especially at the first and second bending vibrating modes of the tower of the WT; (c) The energy radiated by a vibrating WT travels mainly as surface waves with cylindrical spreading and (d) For a WT farm consisting of a number N of WTs the seismic contribution is $\sqrt{N}$ times the contribution of one WT. Widmer-Schnidrig et al. [43], reported that seismic waves generated by a WT are propagating at 2.5 Hz with a geometrical decay of order $O(1/r^2)$, while at 9.5 Hz and 12.5 Hz they attenuate as $O(1/r)$ and $O(1/r^{o0.5})$, respectively. An important work on the subject is that of Stammler and Ceranna [35] reporting signals captured by the seismometers of the Gräfenberg array in Germany before and after the installation of WTs in the area. The most interesting conclusions of their observations are: (a) WTs installed up to 7 km from the Gräfenberg array produce significant vibration energy in a frequency range 1–7 Hz; (b) Signals at 1.15 Hz are detectable in distances more that 15 km from the WT and their strength do not show a consistent decay and spreading pattern and (c) The stronger the wind the stronger the signals captured at the frequencies 1–7 Hz. The results of Stammler and Ceranna [35] confirm the corresponding results taken by Saccorotti et al. [34]. Finally, very interesting information on the imposed moment on the foundation of a vibrating WT can be found in the work of Ishii and Ishihara [11]. More precisely, they report that for a wind speed 9 m/s, the pitch angle remains at 0 degree so that the WT can maximize its power production. In that case, the change of tower base moment

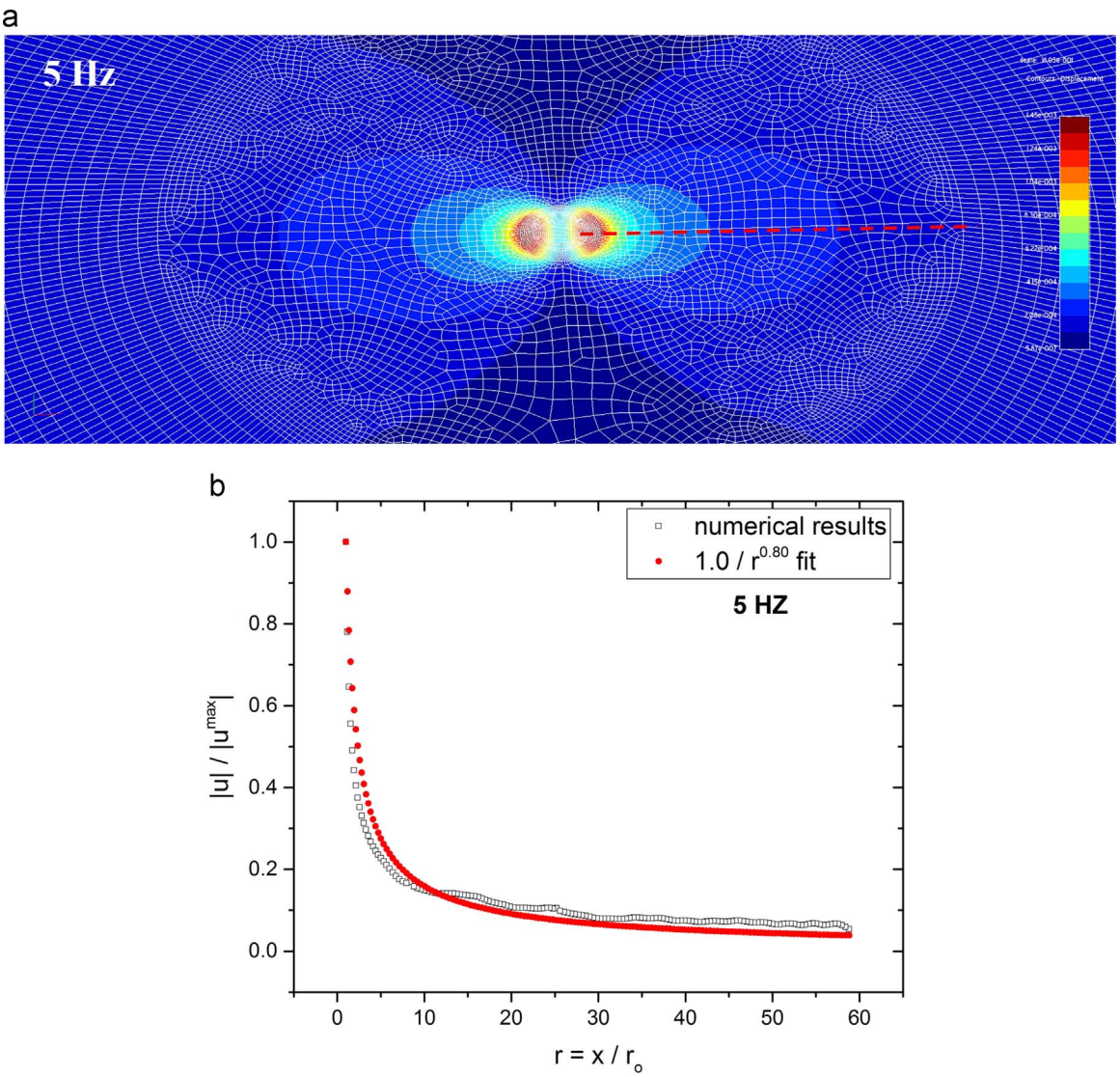

Fig. 7. The same as in Fig. 6 for the frequency of 5 Hz. In the line shown in Fig. 4(a), the vertical displacement of the soil decays as $1/r^{0.8}$.

follows the change in wind speed as happens to other civil structures. At the wind speed of 15 m/s, large and sudden decreases in the pitch angle are observed when the wind speed decreases and the maximum base moment is recorded when the pitch angle sudden increases following the increase of wind speed. According to Ishii and Ishihara [11] the frequency of those changes is very low and between 0.1 Hz and 0.4 Hz, while for a 2 MW WT the base moments of the vibrating tower are between 10MNm and 20MNm. For 5 MW WTs the base bending moment, under extreme conditions, can be greater than 120 MNm [30]. In the present work, utilizing a simplified beam model we evaluated a base bending moment of 78.202 MNm. That moment is used in the present work as the amplitude of the harmonic excitation acting on the above side of the considered foundation.

Taking into account the aforementioned information, the 3D problems of a WT's circular foundation (Fig. 2) subjected to harmonic vertical, shear and bending excitations at 1 Hz, 5 Hz and 10 Hz are solved numerically via the ACA/BEM code explained in the previous section. The foundation of the WT is made by concrete while the density, the Young modulus and the Poisson ratio for both soil and concrete are given in Table 2. A damping ratio of 2% has been assumed for the soil.

3.1. Radiated waves by the vertical motion of the WT

First we consider the vertical (axial) vibration mode of the WT. The vertical harmonic force applying on the top of the cylindrical foundation of the WT, corresponding to base bending moment of 78.202 MNm, has been found equal to N = 178 kN. That force corresponds to a uniformly distributed traction field of amplitude t = 1.180 kPa. The problem has been solved in frequency domain for the low frequencies of 1 Hz, 5 Hz and 10 Hz, while 92,063 linear elements have been utilized for the discretization of the free surface of the soil. The vertical displacement of the free soil surface at a radius of 700 m from the WT as well as the corresponding geometrical attenuation of the generated surface waves are depicted in Figs. 3, 4 and 5, respectively.

From Figs. 3,4 and 5 it is apparent that the generated seismic waves

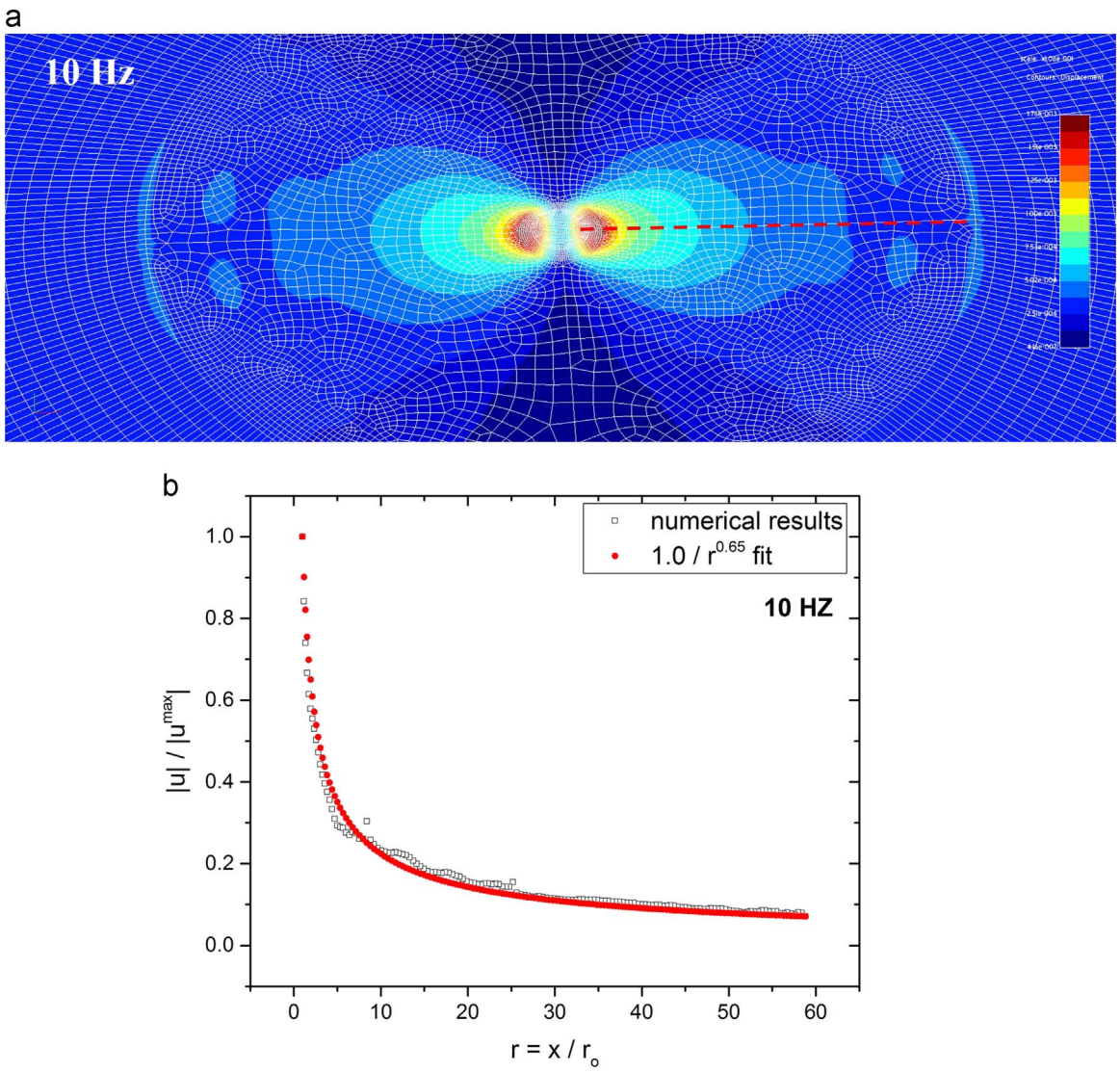

Fig. 8. The same as in Fig. 3 for the frequency of 10 Hz. In the line shown in Fig. 4(a), the vertical displacement of the soil decays as $1/r^{0.65}$.

spread uniformly to all directions because of the axisymmetry of the problem. The waves generated at 1 Hz excitation exhibit an amplitude decay of $1/r$, while the harmonic excitations of 5 Hz and 10 Hz produces waves propagating almost as Rayleigh waves decaying as $1/\sqrt{r}$.

3.2. Radiated waves by the bending vibrational motion of the WT

Next we consider the bending vibrational modes of the WT, which impose a base moment of M = 78.202 MNm at the top of the circular foundation. As it has been already mentioned, this value represents an extreme loading condition for a 5 MW WT. As in the case of axial vibrations, the present problem is solved with 92,063 linear elements and for the low frequencies of 1 Hz, 5 Hz and 10 Hz. The harmonic vertical displacement at the free surface of the soil up to 700 m far from the WT and the corresponding geometrical attenuation of the generated surface waves are depicted in Figs. 6,7 and 8, respectively.

As it is expected the behavior in Figs. 6, 7 and 8 is different to that shown in Figs. 3, 4 and 5 since, due to bending moments, the generated seismic waves spread in the free surface of the soil as a dipole. The harmonic excitation of 1 Hz leads to waves propagating as body waves in the free surface of a half-space decaying as $1/r^2$, while the frequencies of 5 Hz and 10 Hz derive waves decaying as $1/r^{0.8}$ and $1/r^{0.65}$, respectively.

3.3. Radiated waves by the horizontal vibrations of the WT

Finally, we consider the horizontal vibration of the WT, which according to the loading case of bending moment 78.202MN imposes a parallel to the soil dynamic force of amplitude N = 976.0 kN resulting to a uniformly distributed shear traction field of t = 6.469 kPa applied on the top of the circular foundation of the WT. The problem is solved in frequency domain for the low frequencies 1 Hz, 5 Hz and 10 Hz and the vertical displacement of the free soil surface up to 700 m far from the WT as well as the corresponding geometrical attenuation of the

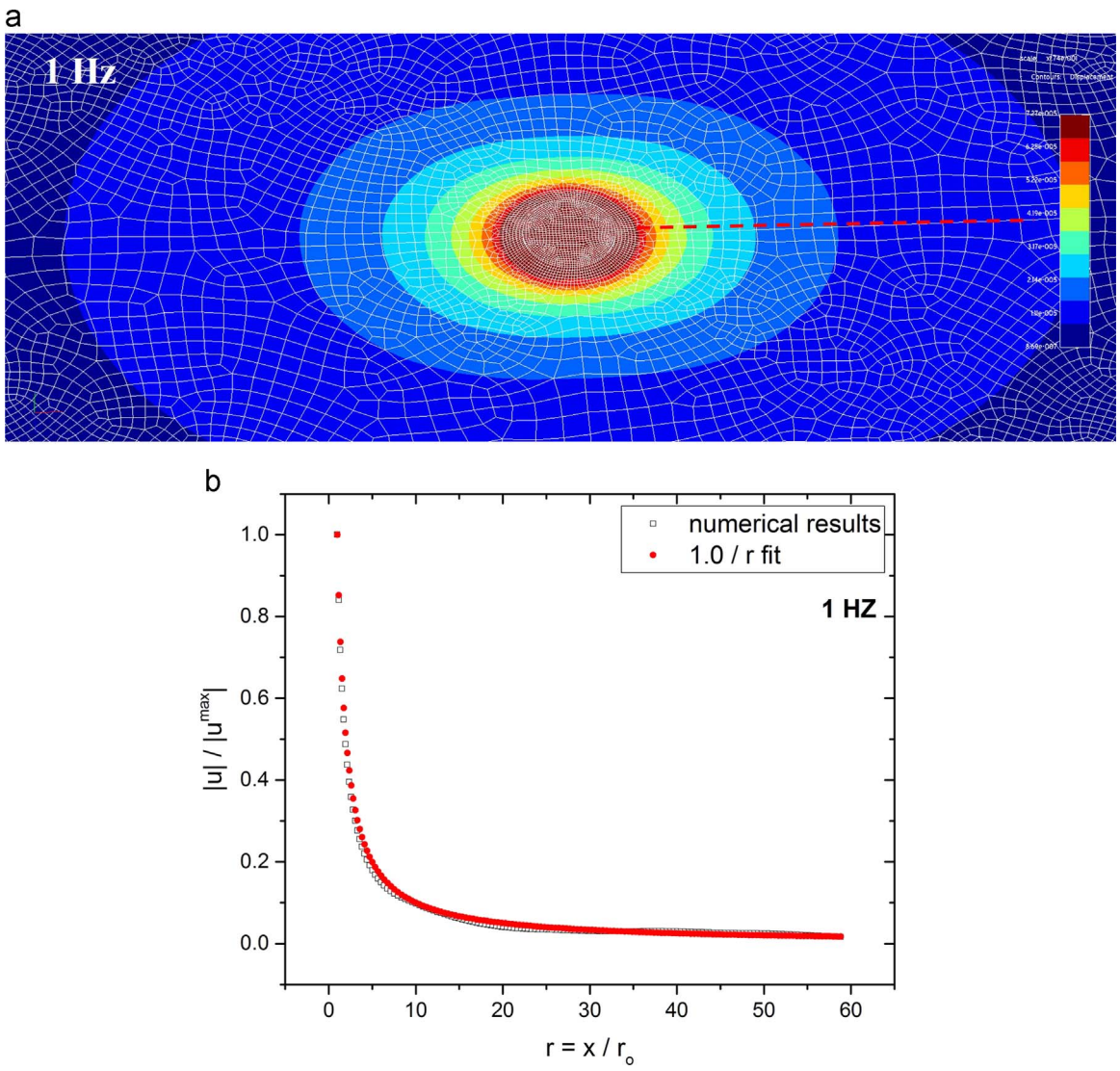

Fig. 9. (a) Contour map of horizontal displacements around the WT's foundation derived by a horizontal traction loading of at the frequency of 1 Hz. (b) The decay of vertical displacements normalized by the maximum displacement appearing at the soil-foundation interface versus radial distance r. The horizontal distance from the WT is normalized by the radius of the foundation $r_o = d_a/2$. In the line shown in Fig. 9(a), the vertical displacement of the soil decays as $1/r$.

generated surface waves are depicted in Figs. 9,10 and 11, respectively. For all frequencies the problem is solved with 92,063 linear elements corresponding to 90,360 nodes.

Figs. 9, 10 and 11 reveal that the vertical disturbances of the free surface of the soil propagate in an elliptical way with faster waves being those corresponding to the direction of the applied horizontal, shear traction. Their attenuation seems to be the same for all the harmonic excitations since in the line being parallel to the considered shear forces the 1 Hz propagating wave decays as $1/r$, while the frequencies of 5 Hz and 10 Hz derive waves both decaying as $1/r^{0.9}$. Utilizing the decay relation $A_2/A_1 = (r_1/r_2)^n$ with A_1, A_2 being the displacements at distances r_1, r_2, respectively, from of the foundation at the line illustrated in Figs. 3(a)–11(a) and n the corresponding decay factor, one obtains the Table 1. The displacement value at the distance of 300 m has been evaluated via our BEM analysis, while the other values have been calculated with the aforementioned analytical decay relation, with the exponential coefficient n obtaining the values based on the polynomial fittings of Figs. 3–11.

The main conclusions of the present section can be summarized as follows

(i) Most of the seismic waves generated by the vibrations of a WT spread as Rayleigh waves, a result that confirms the observations of Styles and co-workers. Taking into account that the low frequency aerodynamic acoustic noise radiated by a WT spreads as cylindrical wave [18], one can say that both acoustic and elastic wave propagation problems associated with the vibration of a WT can be simulated through 2D considerations as a first approximation without significant error and with high computational gain.
(ii) Far away from the WT the results show that bigger disturbances are generated at the of 5 Hz and 10 Hz.
(iii) The very low frequency seismic waves (up to 2 Hz) coming from the bending vibrations of a WT, decay very fast in contrary to those generated by the axial mode of the vibrating WT, which decay as

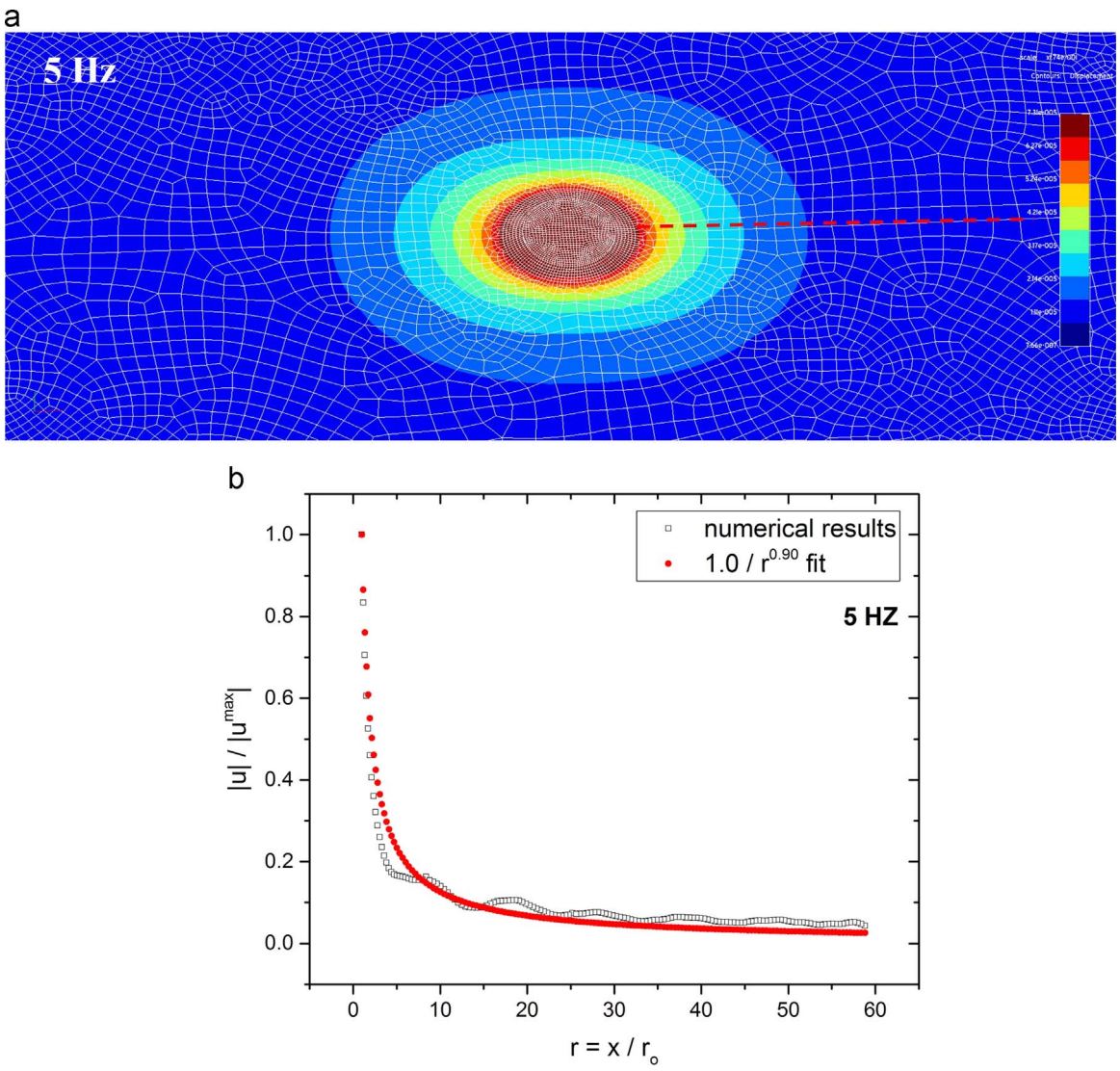

Fig. 10. The same as in Fig. 9 for the excitation frequency of 5 Hz. In the line shown in Fig. 10(a), the vertical displacement of the soil decays as $1/r^{0.9}$.

$1/r$ and can be detected at long distances. Besides, as it is pointed out by Ishii and Ishihara [11], the sudden changes by the pitch control creates significant low frequency axial loading on the foundation of a WT. Perhaps the action of those axial forces explains the very low frequency disturbances detected at long distances reported in the works of Rushforth et al. [31,32], Styles et al. [36,37], Saccorotti et al. [34] and Stammler and Ceranna [35].

(iv) Knowing that seismological centers like those of Eskdalemuir in Scotland and Gräfenberg in Germany are sensitive in wave displacements below to 1 nm, it is apparent from Table 1 that the nearest WT farm should be located at least 15 km away from them. For a wind farm consisting of N WTs the above results are enhanced $\sqrt{N}$ times [36]. This observation enhance the previous conclusion and confirm the suggestion of Stammler and Ceranna [35] that the nearest WT farm should be 50 km away from a seismological center.

(v) According to Klæboe and Fyhri [17] and Woodcock et al. [44], people report different degrees of annoyance with respect to the velocity of the vibrations in their living place. For example the vibration velocity of 0.001 m/s corresponds to disturbances, which are highly annoyed for 15% of asked people and noticeable by the rest 85%. That velocity corresponds to vibration amplitudes of 1.59×10^{-4} m, 3.18×10^{-5}m and 1.59×10^{-5} m for the frequencies 1 Hz, 5 Hz and 10 Hz, respectively. Observing the amplitudes given in Table 1, it is apparent that vibrations coming from the bending modes of the WT at the frequencies of 5 Hz and 10 Hz seem to be very noticeable up to 500 m far from the WT.

4. Acoustic noise radiated by a WT: 2D simulations

As it has been already mentioned in the introduction, WTs generate noise and vibrations, which propagate principally through the air and ground, respectively and due to air-soil interaction the propagating

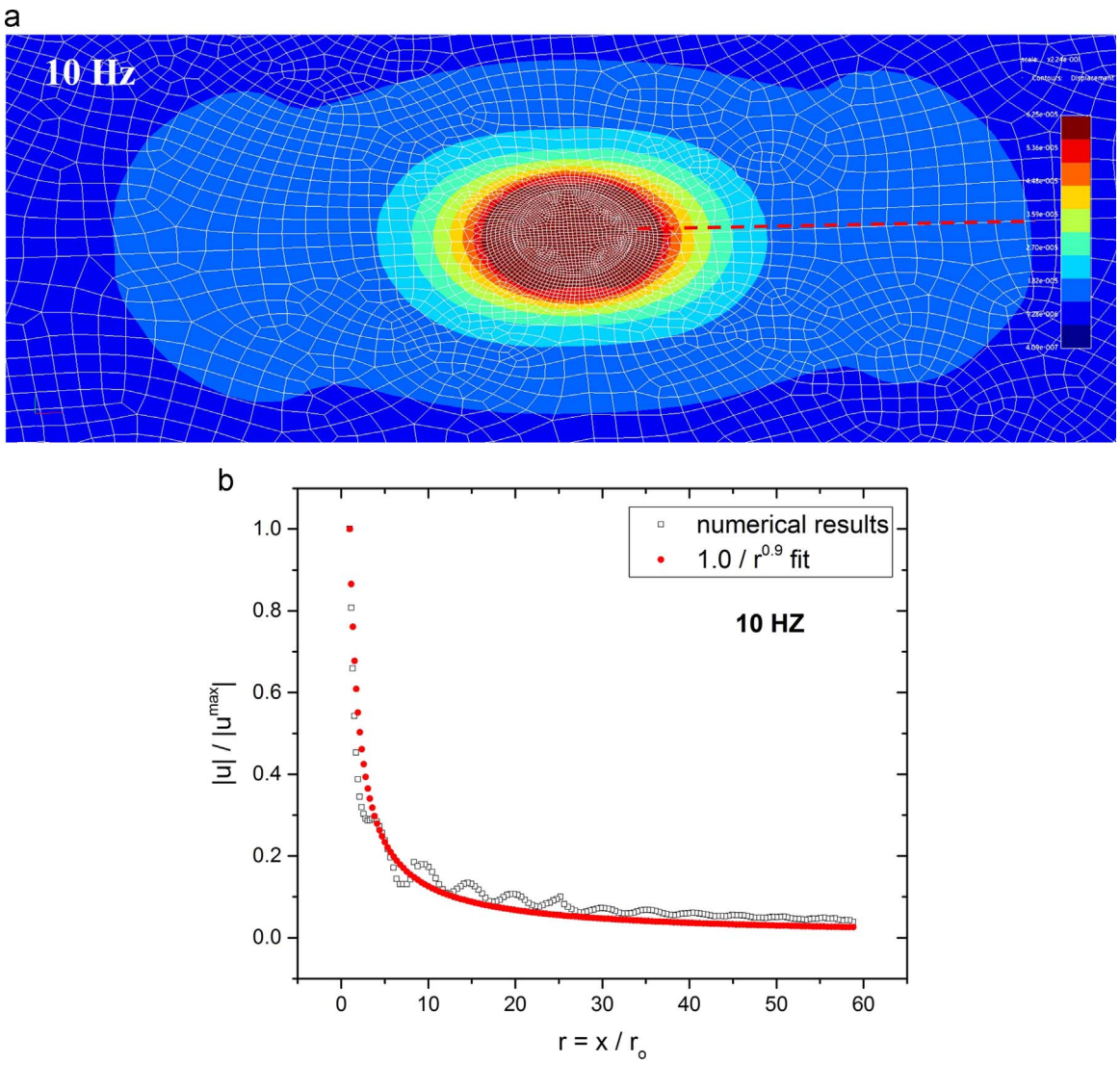

Fig. 11. The same as in Fig. 3 for the excitation frequency of 10 Hz. In the line shown in Fig. 11(a), the vertical displacement of the soil decays as $1/r^{0.9}$.

energy either dives into the soil or refloat to the atmosphere. The goal of the present section is to examine numerically the effect of both acoustic and seismic noise to a structure located 500 m far from a WT. In the previous section we have seen that seismic waves at 5 Hz and 10 Hz generated by the vibrations of a WT spread as cylindrical waves, while the very low frequency surface waves of 1 Hz admit a higher geometric attenuation. On the other hand, acoustic waves generated aerodynamically by a WT propagate, after a critical distance from the WT, as cylindrical waves with a geometrical attenuation being smaller than that of spherical waves [18]. All this information leads to the conclusion that 2D numerical predictions for ground and airborne noise generated by a WT are not far from the reality and obviously less expensive than 3D simulations of the same problem. Consequently, the aim of the present section is to provide information on the aforementioned low frequency noise from WTs by solving numerically the 2D fluid-structure interaction problem depicted in Fig. 12. All the geometrical details and material properties of the model are provided in Table 2.

A harmonic monopole acoustic source of pressure amplitude P = 0.3 Pa is considered at the top of the tower of the WT (H_1 = 150 m). The amplitude of the source has been chosen such that the sound pressure level of the source is 83.5 dB and at 500 m far from the source, at the frequency of 10 Hz the sound pressure level is 54.8 dB, taking into account the adopted material properties and the decay of the pressure field of the acoustic source. The foundation of the WT is subjected to a vertical, horizontal and bending loading represented by the forces N = 6.93 kN/m, Q = 1.10 kN/m and the bending moment M = 270 KNm/m, respectively. The values of N, Q and M have been chosen to produce elastic wave displacements of the same order with those calculated in the 3D simulations of the previous section without the presence of the building.

The just described frequency domain fluid-structure interaction problem is solved numerically via the ACA/BEM technique, illustrated in Section 2 and for the low frequencies of 1 Hz, 5 Hz and 10 Hz. The size of the line elements used for the discretization of boundaries and interfaces has been chosen 0.2 m, which corresponds to 165 quadratic

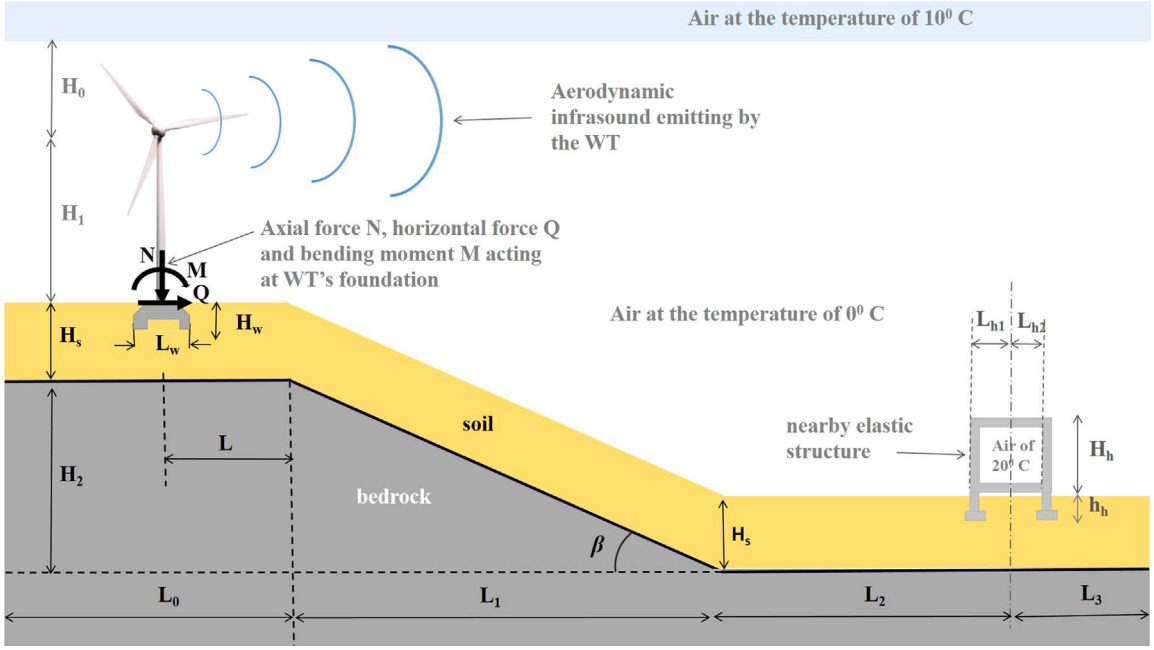

Fig. 12. Geometry and materials for the 2D model used in the numerical simulation for the propagation of infrasound and micro-seismic waves generated by a WT.

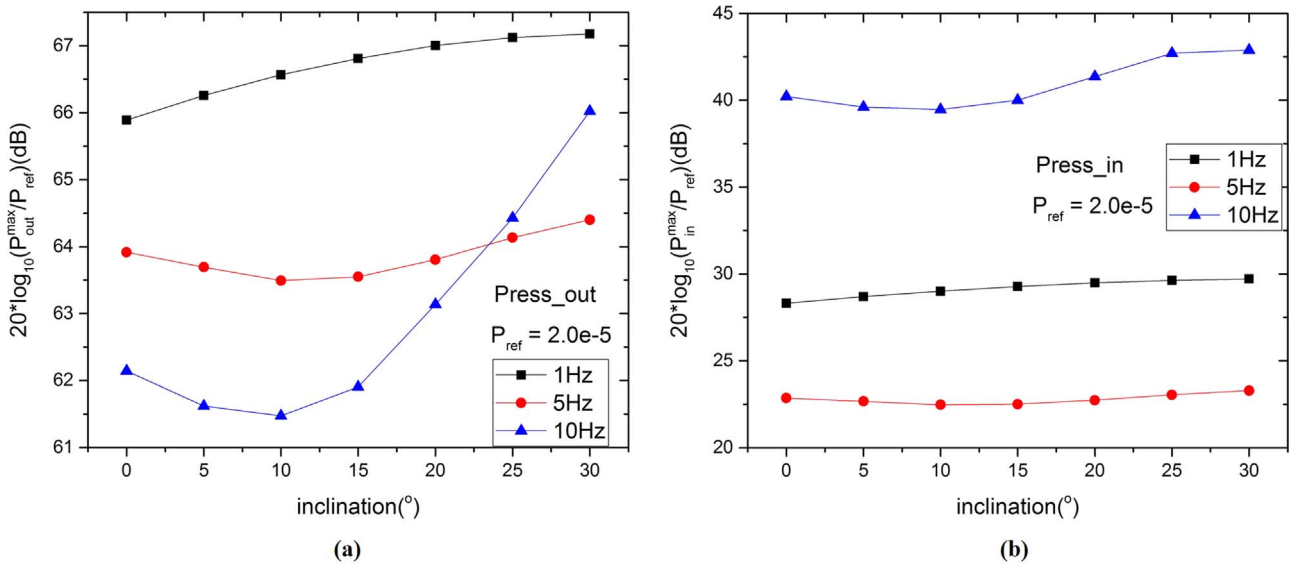

Fig. 13. The maximum values of the sound pressure level (a) inside and (b) outside of the structure located 500 m far from the WT for different inclination angles β and for the low frequencies 1 Hz, 5 Hz and 10 Hz. The presented sound is airborne noise coming from the harmonic point monopole source located at the top of the WT, shown in Fig. 12.

elements per wave length of the 10 Hz excited waves in the acoustic region of air at 0 °C. First, the problem where only the acoustic source of the WT is taken into consideration is solved. Fig. 13 represents the maximum values of the sound pressure level inside and outside of the structure located 500 m far from the WT with respect to the inclination angle β. As reference pressure the value of p = 20 μPa is considered. It is apparent that the maximum sound pressure level inside the structure is almost the half in dBs compared to the corresponding maximum value outside the structure. The sound level is higher at the frequency of 1 Hz outside the building while inside the building the sound pressure level is higher for the frequency of 10 Hz. The contribution of the inclination to the sound pressure level is more pronounced for the frequencies of 1 Hz and 5 Hz. Considering the atmosphere as two layers of air at the temperatures of 0 °C and 10 °C with the warmer being that laying above to the WT (Fig. 12) no significant changes at the maximum values of the pressure outside and inside of the structure are observed (Fig. 14).

In the sequel the problem of Fig. 12 is solved by considering only the source of micro-seismic noise, which is the action of the vertical and horizontal forces N and Q, respectively and the bending moment M. Fig. 15 demonstrates the maximum acoustic pressure levels inside and

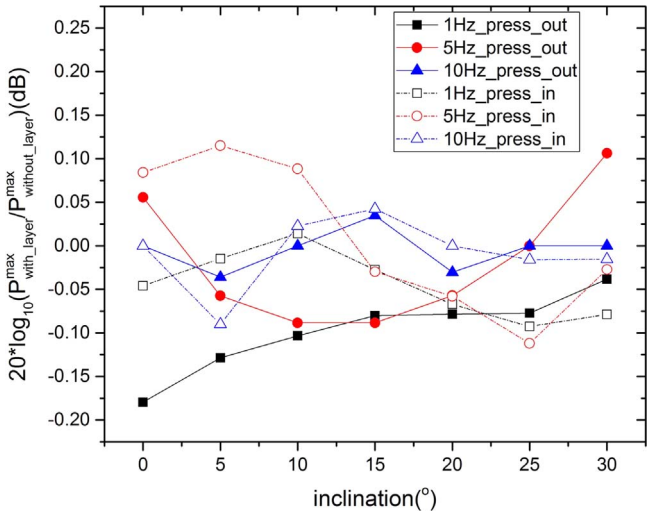

Fig. 14. Contribution of a warmer layer of air above to the WT on the sound pressure level inside (dashed lines) and outside (continuous lines) of the considered structure for different inclination angles β.

outside of the structure for the acoustic noise generated by the micro-seismicity and the coupling between air, soil and structure. The reference pressure is considered again 20μPa and the contribution of the inclination angle β has been taken into account. An important remark is that micro-seismicity is able to produce acoustic noise, which is almost the same inside and outside to the structure. Furthermore the noise level is higher for the frequency of 10 Hz. Solving the same problem with the presence of bedrock, shown in Fig. 12, one can see in Fig. 16 that for all frequencies the bedrock has an additional contribution to the generated acoustic noise, with more pronounced contribution being at 1 Hz. For higher frequencies of 5 Hz or 10 Hz the thickness of the soil above the rock is 2–3 times greater than the wave length. Therefore the surface tremors are not affected so much by the rock presence, considering also the fact that the soil acts as a kind of low pass filter. Comparing Figs. 13(a) and 15(a), 16(a), we reach to the important conclusion that seismic waves generate greater levels of noise inside the structure than those produced by the propagating airborne noise.

5. Conclusions

The Boundary Element Method (BEM) has been employed for the solution of 2D and 3D problems dealing with the airborne and ground borne low frequency noise produced by a wind turbine (WT). All the simulations have been performed in frequency domain and for the frequencies of 1 Hz, 5 Hz and 10 Hz. Both air and soil has been implemented as linear materials and their air-soil interaction has been taken into account. Since all the obtained results are taken through linear models, any increase in the acoustic and elastic wave excitation is automatically reflected to the evaluated pressures and displacements, respectively. For this reason all the presented here results are given in dBs without using A, B or G filters. First the micro-seismic waves generated by the bending, vertical and horizontal vibrations of a WT have been examined through 3D simulations and their decay rate in dependence with the distance from the vibrating WT has been assessed. The interesting conclusions extracted by those simulations are: (i) most of the seismic waves generated by the vibrations of a WT spread as Rayleigh waves; (ii) the generated microseismic waves affect the measurements of seismological centers located even 15 km far from a WT farm; (iii) bigger disturbances are produced at the frequency range of 5–10 Hz and (iv) the operation of a WT under strong winds generates microseismic waves that would cause annoyance for the neighbors. Since airborne and soil borne noise produced by a WT propagate as cylindrical and Rayleigh waves, respectively, 2D simulations of that fluid-structure interaction problem have been performed for a specific geometry and a structure located 500 m far from the WT. The most important conclusions here are (i) the microseismicity creates higher levels of noise inside a house than that of the airborne noise radiated by a WT and (ii) bedrock being in low depths underneath the soil has an additional contribution to the generated acoustic noise by the induced microseismicity.

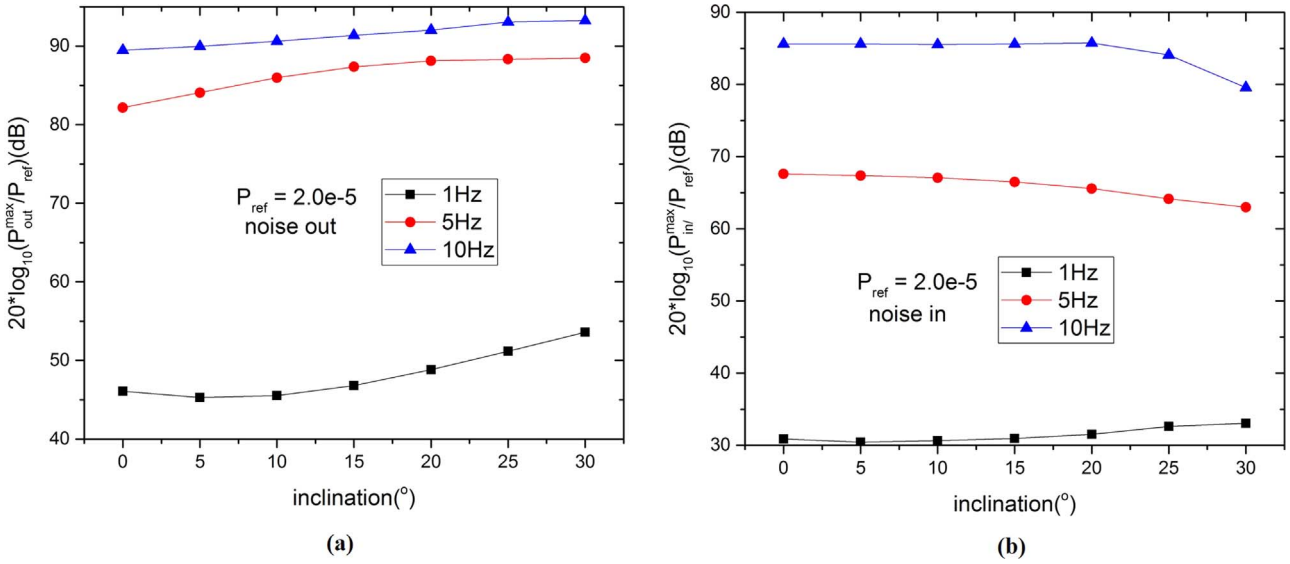

Fig. 15. The maximum values of the sound pressure level (a) inside and (b) outside of the structure located 500 m far from the WT for different inclination angles β and for the low frequencies 1 Hz, 5 Hz and 10 Hz. The presented here sound level is due to the micro-seismic waves generated by the vibrations of the WT and the coupling between the air and the vibrating soil.

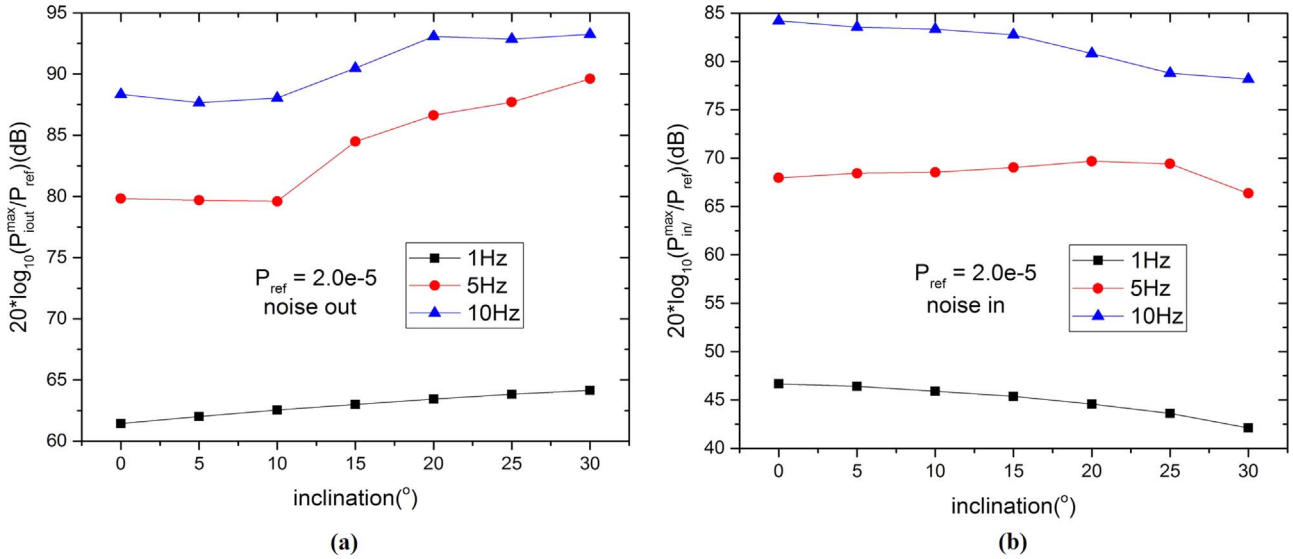

Fig. 16. The same as in Fig. 15 with the soil being a 100 m layer supporting by bedrock as it is illustrated in Fig. 12.

Acknowledgements

This work is part of the work package "Wave Propagation and Dynamic Soil-Structure Interaction" of the joint research project "Objective Criteria for Seismic and Acoustic Emission of Inland Wind Turbines (TremAc), FKZ 0325839A", funded by the German Federal Ministry for Economic Affairs and Energy (BMWi). The authors are grateful to BMWi for the financial support.

References

[1] Abbasi T, Premalatha M, Abbasi T, Abbasi SA. Wind energy: increasing deployment, rising environmental concerns. Renew Sustain Energy Rev 2014;31:270–88.
[2] Adewumi G, Nyamayoka LT-E, Inambao F. Reducing infrasound and low frequency noise from wind turbine blades and rotors using ANC. Renew Bioresour 2015;2015 〈http://www.hoajonline.com/journals/pdf/2052-6237-3-3.pdf〉.
[3] Agnantiaris JP, Polyzos D. A boundary element method for acoustic scattering from non-axisymetric and axisymmetric elastic shells. CMES: Comput Model Eng Sci 2003;4(1):197–212.
[4] Al-Bahadly, I. (Ed.). Wind Turbines, Published by InTech, Croatia; 2011.
[5] Aliabadi MH. The boundary element method, Volume 2: applications in solids and structures. 2. England: John Wiley; 2002.
[6] Bakker RH, Pedersen E, van den Berg GP, Stewart RE, Lok W, Bouma J. Impact of wind turbine sound on annoyance, self-reported sleep disturbance and psychological distress. Sci Total Environ 2012;425:42–51.
[7] Carman RA. Measurement procedure for wind turbine infrasound, Inter Noise 2015 Conference, San Francisco, California, USA, 9-12 Augaust; 2015.
[8] Gortsas T, Tsinopoulos SV, Polyzos D. An advanced ACA/BEM for solving 2D large-scale problems with multi-connected domains. CMES: Comput Model Eng Sci 2015;107(4):321–43.
[9] Hau E. Wind turbines. Fundamentals, technologies, application, economics. Springer; 2006.
[10] Hoffmeyer D, Jakobsen J. Sound insulation of dwellings at low frequencies. J Low Freq Vib Act Control 2010;29(1):15–23.
[11] Ishii H, Ishihara T. Numerical study of maximum wind load on wind turbine towers under operating conditions, In: Proceedings of the Fifth International Symposium on Computational Wind Engineering (CWE2010), Chapel Hill, North Carolina, USA May 23-27; 2010.
[12] Jakobsen J. Infrasound emission from wind turbines. J Low Freq Vib Act Control 2005;24(3):145–55.
[13] Katinas V, Marčiukaitis M, Tamašauskienė M. Analysis of the wind turbine noise emissions and impact on the environment. Renew Sustain Energy Rev 2016;58:825–31.
[14] Keith SE, et al. Wind turbine sound pressure level calculations at dwellings. J Acoust Soc Am 2016;139(3):1436–42.
[15] Kelley ND, Hemphill RR, Mc Kenna HE. A methodology for assessment of wind turbine noise generation. J Sol Energy Eng 1982;104:112–20.
[16] Klæboe R, Sundfør HB. Windmill Noise Annoyance, Visual Aesthetics, and Attitudes towards Renewable Energy Sources. Int J Environ Res Public Health 2016;13:746–65.
[17] Klæboe R, Fyhri A. People's reaction to vibrations in dwellings from road and rail, TØI report 443/1999, Oslo; 1999.
[18] Makarewicz R. Cylindrical spreading of noise from a wind turbine. J Wind Eng Ind Aerodyn 2016;148:1–5.
[19] Manley DMJP, Styles P, Scott J. Perceptions of the public of low frequency noise. J Low Freq Noise Vib Control 2002;21(1):37–44.
[20] Marcillo O, Arrowsmith S, Blom P, Jones K. On infrasound generated by wind farms and its propagation in low-altitude tropospheric waveguides. J Geophys Res: Atmos. 2016:9855–68. http://dx.doi.org/10.1002/2014JD022821.
[21] Michaud DS, et al. Personal and situational variables associated with wind turbine noise annoyance. J Acoust Soc Am 2016;139(3):1455–66.
[22] Michaud DS, et al. Exposure to wind turbine noise: perceptual responses and reported health effects. J Acoust Soc Am 2016;139(3):1443–54.
[23] Mo J-O, Lee Y-H. Numerical simulation for prediction of aerodynamic noise characteristics on a HAWT of NREL phase VI. J Mech Sci Technol 2011;25(5):1341–9.
[24] Møller H, Pedersen CS. Low-frequency noise from large wind turbines. J Acoust Soc Am 2011;129(6):3727–44.
[25] Oerlemans S, Schepers JG. Prediction of wind turbine noise and validation against experiment, Report NLR-TP-2009–2402; 2009.
[26] Öhlund O, Larsson C. Meteorological effects on wind turbine sound propagation. Appl Acoust 2015;89:34–41.
[27] Pedersen E, van den Berg F, Bakker R, Bouma J. Response to noise from modern wind farms in The Netherlands. J Acoust Soc Am 2009;126(2):634–43.
[28] Pilger C, Ceranna L. The influence of periodic wind turbine noise on infrasound array measurements. J Sound Vib 2017;388:188–200.
[29] Polyzos D, Tsinopoulos SV, Beskos DE. Static and dynamic boundary element analysis in incompressible linear elasticity. Eur J Mech A/Solids 1998;17(3):515–36.
[30] Rahman M, Ong Zhi Chao, Wen Tong Chong Julai, Shin Yee Khoo S. Performance enhancement of wind turbine systems with vibration control: a review. Renew Sustain Energy Rev 2015;51:43–54.
[31] Rushforth I, Styles P, Manley DJMP, Toon S. Microseismic investigation of low frequency vibrations and their possible effects on population. J Low-Freq Noise Vib Act Control 1999;18(3):111–21.
[32] Rushforth I, Moorhouse A, Styles P. An integrated acoustic/Microseismic approach to monitoring low frequency noise & vibration – A case study. Build Acoust 2003;V10(1):77–95.
[33] Saad Y, Schulz MH. GMRES: a generalized minimal residual algorithm for solving nonsymmetric linear systems. SIAM J Sci Stat Comput 1986;7(3):856–69.
[34] Saccorotti G, Piccinini D, Cauchie L, Fiori I. Seismic Noise by Wind Farms: a Case Study from the Virgo Gravitational Wave Observatory, Italy. Bull Seismol Soc Am 2011;101(2):568–78.
[35] Stammler K, Ceranna L. Influence of wind turbines on seismic records of the Gräfenberg array. Seismol Res Lett 2016;87(5):1–7.
[36] Styles P, Stimpson I, Toon S, England R, Wright M. Microseismic and infrasound monitoring of low frequency noise and vibration from wind farms 〈https://docs.wind-watch.org/AEG-Eskdalemuir.pdf〉; 2005.
[37] Styles P, Westwood RF, Toon SM, Buckingham MP, Marmo B, Carruthers B. Monitoring and Mitigation of Low Frequency Noise from Wind Turbines to Protect

Comprehensive Test Ban Seismic Monitoring Stations, In: Proceedings of the Fourth International Meeting on Wind Turbine Noise, Rome Italy 12–14 April 2011; 2011.
[38] Turnbull C, Turner J, Walsh D. Measurement and level of infrasound from wind farms and other sources. Acoust Aust 2012;40(1):45–50.
[39] Van den Berg, G.P. Do wind turbines produce significant low frequency sound levels? In: Proceedings of the 11th International Meeting on Low Frequency Noise and Vibration and its Control, Netherlands; 2011.
[40] Van Renterghem T, Bockstael A, De Weirt V, Botteldooren D. Annoyance, detection and recognition of wind turbine noise. Sci Total Environ 2013;456–457:333–45.
[41] Vavourakis V, Protopappas VIC, Fotiadis DI, Polyzos D. Numerical determination of modal dispersion and AE signal characterization in waveguides through LBIE/BEM and time-frequency analysis. Comput Mech 2008;43(3):431–41.
[42] Wagner S, Bareiβ R, Guidati G. Wind turbine noise. Springer; 1996.
[43] Widmer-Schnidrig R, Forbriger T, Zürn W. Windkraftanlagen als seismische Störquellen [64]. Jahr der Dtsch Geophys Ges Berl Tag Seite2004:541.
[44] Woodcock J, Peris E, Condie J, Sica G, Koziel K, Evans T, Moorhouse A, Steele A, Waddington D. Human Response to Vibration in Residential Environments (NANR209), Technical Report 6: Determination of exposure-response relationships, Defra (London); 2011.
[45] Wrobel LC. The boundary element method, Volume 1: applications in thermo-fluids and acoustics. 1. England: John Wiley; 2002.
[46] Zajamšek B, Hansen KL, Doolan CJ, Colin H, Hansen CH. Characterisation of wind farm infrasound and low-frequency noise. J Sound Vib 2016;370:176–90.